ELECTRONICS AND ELECTRICAL ENGINEERING
ISSN 1392 – 1215 *2010. No. 7(103)*
ELEKTRONIKA IR ELEKTROTECHNIKA

T 121 *SIGNAL TECHNOLOGY*
SIGNALŲ TECHNOLOGIJA

One Method of Image Processing and its Numerical Analysis

A. Lorencs, J. Sinica-Sinavskis
Institute of Electronics and Computer Science,
Dzerbenes st. 14, LV-1006, Riga, Latvia, phone +371 67558192, e–mail: jss@edi.lv

Introduction

The paper is devoted to analysis of digital image processing issues for the case when the linear regression models (LRM) are used for transformation and classification of these images. Using methods of numerical analysis, we will investigate representation precision and classification quality of these images by comparing different representation cases of real digital images. It is expected that more precise representation would ensure higher precision of classification, i.e. lower classification error rate.

Throughout the study, members of Fourier series and their products are used as basis functions of LRM.

In the paper, we will consider grayscale digital images in the form of $m \times n$ matrices of rational numbers each representing brightness level of a pixel from the real scene. All digital images exploited for numerical analysis are obtained by scanning of real scenes with further preprocessing including application of a logarithmic operator and elimination of the background trend on the basis of median filtering. In the same way as in [1], elements of digital image $\mathbf{A} = (a_{ij})$ will be interpreted as applicates (z coordinate values) of a geometric surface $V_{\mathbf{A}}$ that are perturbed by realizations of the random variables X_{ij} with Gaussian distribution. It is assumed that X_{ij} are independent, their mean values are $EX_{ij} = 0$ and variances $DX_{ij} = \sigma^2$ are very small. Therefore we may assume that $a_{ij} \approx z_{ij}$. With such interpretation, we can analytically approximate the surface $V_{\mathbf{A}}$ by means of a relevant LRM

$$f(x, y; \boldsymbol{\theta}) = \sum_{k=0}^{K} \theta_k \varphi_k(x, y), \qquad (1)$$

where $\varphi_k(x, y)$ are basis functions of the LRM, and θ_k are components of an unknown vector $\boldsymbol{\theta}$. Estimate $\hat{\boldsymbol{\theta}}$ of the coefficient vector $\boldsymbol{\theta}$ usually is calculated using the least squares method, i.e. finding it as a minimum point of a function

$$Q(\boldsymbol{\theta}) = \sum_{i=1}^{m} \sum_{j=1}^{n} (a_{ij} - f(x_i, y_j; \boldsymbol{\theta}))^2 . \qquad (2)$$

Argument values of the functions x_i and y_j will be determined accordingly with the chosen basis functions and calculated for each pair of indices (i, j) using the certain formula.

Analytic approximation of the geometric surface $V_{\mathbf{A}}$ can be performed also in a different way, namely by transforming the digital image $\mathbf{A} = (a_{ij})$ into a $m \cdot n$ dimensional vector $\boldsymbol{\alpha} = (a_{11}, a_{12}, ..., a_{1n}, a_{21}, a_{22}, ..., a_{2n}, ..., a_{m1}, a_{m2}, ..., a_{mn})^T$. In this case, applicates z_{ij} of discrete points of $V_{\mathbf{A}}$ turn into ordinates of a geometric curve $L_{\mathbf{A}}$. Analytic approximation of $L_{\mathbf{A}}$ can be found using the relevant LRM as

$$g(x; \boldsymbol{\theta}) = \sum_{k=0}^{K} \theta_k \varphi_k(x). \qquad (3)$$

Estimate $\hat{\boldsymbol{\theta}}$ of a vector $\boldsymbol{\theta}$ of unknown coefficients θ_k is calculated again using the least squares method by finding it as a minimum point of a function

$$\tilde{Q}(\boldsymbol{\theta}) = \sum_{i=1}^{m} \sum_{j=1}^{n} (a_{ij} - g(x_{ij}; \boldsymbol{\theta}))^2 . \qquad (4)$$

If the number of basis functions of LRM (1) and LRM (2) is the same, it is expected that analytic approximations of $V_{\mathbf{A}}$ will be close. However, results of numerical analysis show that such hypothesis is controversial.

In order to ensure fast calculation of estimates $\hat{\boldsymbol{\theta}}$, a relatively small number of basis functions was chosen in all LRMs (if compared with $m \cdot n$). That guarantees non-

singularity of the matrix $\mathbf{M}=\mathbf{F}^T\mathbf{F}$ and, consequently, possibility to calculate $\hat{\boldsymbol{\theta}}$ according to formula

$$\hat{\boldsymbol{\theta}}=\mathbf{M}^{-1}\mathbf{F}^T\boldsymbol{\alpha}, \tag{5}$$

where $\mathbf{F}$ is the design matrix of the corresponding model with elements $\varphi_k(x_i,y_j)$ or $\varphi_k(x_{ij})$. If ν_{ij} is the order number of a component a_{ij}, then the ν_{ij}-st row of a design matrix is a vector $\langle\varphi_0(x_i,y_j),\varphi_1(x_i,y_j),...,\varphi_K(x_i,y_j)\rangle$. In the case of model (2), this row of the matrix $\mathbf{F}$ will be a vector $\langle\varphi_0(x_{ij}),\varphi_1(x_{ij}),...,\varphi_K(x_{ij})\rangle$.

Thus, the calculation of estimates $\hat{\boldsymbol{\theta}}$ for different images $\mathbf{A}$ is done by replacing only the vector $\boldsymbol{\alpha}$ in formula (3).

Approximation precision of digital images

Let us discuss digital images represented by matrices 25×25 that correspond to certain categories of real scenes. We had a number of digital images at our disposal, obtained from two different categories of real scenes: scenes where small metal rings (category 1) and pieces of glass (category 2) were eventually present. Sizes of digital images were chosen in a way ensuring that eventually present foreign body (ring or glass) is fully contained in such fragment.

Model (1) uses products of members of Fourier series $\varphi_s(x)$, $\varphi_t(y)$ as basis functions $\varphi_k(x,y)$. Model (2) uses basis functions $\varphi_0(x)=1$, $\varphi_1(x)=\cos x$, $\varphi_2(x)=\sin x$, $\varphi_3(x)=\cos 2x$, $\varphi_4(x)=\sin 2x$, etc. System of basis functions of model (1) is arranged according to the following principle [2]:

$\varphi_{s'}(x)\cdot\varphi_{t'}(y)$ follows the $\varphi_s(x)\cdot\varphi_t(y)$, if

1) $\max(s',t')>\max(s,t)$;
2) $\max(s',t')=\max(s,t)$ and $s'+t'>s+t$;
3) $\max(s',t')=\max(s,t)$, $s'+t'=s+t$ and $s<s'$.

According to the assumed principle, the first 9 members of functions $\varphi_k(x,y)$ form a functional vector $\langle 1,\cos y,\cos x,\cos x\cdot\cos y,\sin y,\sin x,\cos x\cdot\sin y,$ $\sin x\cdot\cos y,\sin x\cdot\sin y\rangle$. The first twenty-five (resp., forty-nine) functions are presented in Table 1. Further we shall use numerical analysis to evaluate three different cases of models (1) and (2), assuming that the first case V_1 relates to number of basis functions K_1+1, the second case V_2 - to K_2+1 and the third case V_3 - to K_3+1, where $K_1=8$, $K_2=24$ and $K_3=48$.

Table 1. Two argument trigonometric basis functions

No.	Basis functions	No.	Basis functions
1	1	26	cos(3 *y*)
2	cos(*y*)	27	cos(3 *x*)
3	cos(*x*)	28	cos(*x*) cos(3 *y*)
4	cos(*x*) cos(*y*)	29	cos(3 *x*) cos(*y*)
5	sin(*y*)	30	sin (*x*) cos(3 *y*)
6	sin(*x*)	31	cos(3 *x*) sin(*y*)
7	cos(*x*) sin(*y*)	32	cos(2 *x*) cos(3 *y*)
8	sin (*x*) cos(*y*)	33	cos(3 *x*) cos(2 *y*)
9	sin (*x*) sin(*y*)	34	sin (2 *x*) cos(3 *y*)
10	cos(2 *y*)	35	cos(3 *x*) sin(2 *y*)
11	cos(2 *x*)	36	cos(3 *x*) cos(3 *y*)
12	cos(*x*) cos(2 *y*)	37	sin(3 *y*)
13	cos(2 *x*) cos(*y*)	38	sin (3 *x*)
14	sin (*x*) cos(2 *y*)	39	cos (*x*) sin (3 *y*)
15	cos(2 *x*) sin(*y*)	40	sin(3 *x*) cos(*y*)
16	cos(2 *x*) cos(2 *y*)	41	sin (*x*) sin(3 *y*)
17	sin(2 *y*)	42	sin(3 *x*) sin(*y*)
18	sin (2 *x*)	43	cos(2 *x*) sin(3 *y*)
19	cos (*x*) sin (2 *y*)	44	sin(3 *x*) cos(2 *y*)
20	sin(2 *x*) cos(*y*)	45	sin(2 *x*) sin(3 *y*)
21	sin (*x*) sin(2 *y*)	46	sin(3 *x*) sin(2 *y*)
22	sin(2 *x*) sin(*y*)	47	cos (3 *x*) sin(3 *y*)
23	cos(2 *x*) sin(2 *y*)	48	sin(3 *x*) cos(3 *y*)
24	sin(2 *x*) cos(2 *y*)	49	sin(3 *x*) sin(3 *y*)
25	sin(2 *x*) sin(2 *y*)		

The following models will be considered then

$$f_1(x,y;\boldsymbol{\theta})=\sum_{k=0}^{8}\theta_k\varphi_k(x,y), \tag{6}$$

$$f_2(x,y;\boldsymbol{\theta})=\sum_{k=0}^{24}\theta_k\varphi_k(x,y), \tag{7}$$

$$f_3(x,y;\boldsymbol{\theta})=\sum_{k=0}^{48}\theta_k\varphi_k(x,y), \tag{8}$$

$$g_1(x;\boldsymbol{\theta})=\sum_{k=0}^{8}\theta_k\varphi_k(x), \tag{9}$$

$$g_2(x;\boldsymbol{\theta})=\sum_{k=0}^{24}\theta_k\varphi_k(x), \tag{10}$$

$$g_3(x;\boldsymbol{\theta})=\sum_{k=0}^{48}\theta_k\varphi_k(x). \tag{11}$$

Taking into account the character of basis functions and the size of digital images, values x_i and y_j of arguments x and y were determined according to

$$x_i=2\pi\cdot\frac{i-13}{25}, \tag{12}$$

$$y_j=2\pi\cdot\frac{j-13}{25}, \tag{13}$$

$$x_{ij}=2\pi\cdot\frac{\nu_{ij}-313}{625}. \tag{14}$$

It follows directly from the equalities (7), (8), (9) that, for the model (1), values of basis functions will be calculated within the square $[-\pi,\pi]\times[-\pi,\pi]$, and for the model (2), within the interval $[-\pi,\pi]$.

Taking into account the fixed number of basis functions in LRMs ((6), (7), (8), (9), (10), (11)), it is easy to be convinced that matrixes $\mathbf{M}$ for all models will be non-singular. Therefore transformation of digital images into the estimates $\hat{\boldsymbol{\theta}}$ can be performed using the formula (3).

Three different measures are chosen for the evaluation of precision of analytical approximation: $R_1\left(\mathbf{A}, M_{\mu,\nu}\right)$, $R_2\left(\mathbf{A}, M_{\mu,\nu}\right)$ and $R_3\left(\mathbf{A}, M_{\mu,\nu}\right)$, where $\mu = \overline{1,2}$, $\nu = \overline{1,3}$. Precision measure $R_1\left(\mathbf{A}, M_{\mu,\nu}\right)$ for the model (1) is defined by the equality

$$R_1\left(\mathbf{A}, M_{1,\nu}\right) = \sqrt{\sum_{i=1}^{25}\sum_{j=1}^{25}\left(a_{ij} - f_\nu\left(x_i, y_j; \hat{\boldsymbol{\theta}}\right)\right)^2}, \quad (15)$$

for the model (2) - by the equality

$$R_1\left(\mathbf{A}, M_{2,\nu}\right) = \sqrt{\sum_{\nu_{ij}=1}^{625}\left(a_{ij} - g_\nu\left(x_{ij}; \hat{\boldsymbol{\theta}}\right)\right)^2}. \quad (16)$$

Precision measure $R_2\left(\mathbf{A}, M_{\mu,\nu}\right)$ for the model (1) is defined by the equality

$$R_2\left(\mathbf{A}, M_{1,\nu}\right) = \frac{\boldsymbol{\alpha}^T\boldsymbol{\beta}}{\boldsymbol{\alpha}^T\boldsymbol{\alpha} + \boldsymbol{\beta}^T\boldsymbol{\beta} - \boldsymbol{\alpha}^T\boldsymbol{\beta}}, \quad (17)$$

where $\boldsymbol{\beta} = \left(f_\nu\left(x_1, y_1; \hat{\boldsymbol{\theta}}\right), f_\nu\left(x_1, y_2; \hat{\boldsymbol{\theta}}\right), \ldots, f_\nu\left(x_1, y_{25}; \hat{\boldsymbol{\theta}}\right), f_\nu\left(x_2, y_1; \hat{\boldsymbol{\theta}}\right), f_\nu\left(x_2, y_2; \hat{\boldsymbol{\theta}}\right), \ldots, f_\nu\left(x_2, y_{25}; \hat{\boldsymbol{\theta}}\right), \ldots, f_\nu\left(x_{25}, y_1; \hat{\boldsymbol{\theta}}\right), f_\nu\left(x_{25}, y_2; \hat{\boldsymbol{\theta}}\right), \ldots, f_\nu\left(x_{25}, y_{25}; \hat{\boldsymbol{\theta}}\right)\right)^T$.

For models (2), this measure of similarity of Tanimoto type will be defined as follows

$$R_2\left(\mathbf{A}, M_{2,\nu}\right) = \frac{\boldsymbol{\alpha}^T\boldsymbol{\gamma}}{\boldsymbol{\alpha}^T\boldsymbol{\alpha} + \boldsymbol{\gamma}^T\boldsymbol{\gamma} - \boldsymbol{\alpha}^T\boldsymbol{\gamma}}, \quad (18)$$

where $\boldsymbol{\gamma} = \left(g_\nu\left(x_{1,1}; \hat{\boldsymbol{\theta}}\right), g_\nu\left(x_{1,2}; \hat{\boldsymbol{\theta}}\right), \ldots, g_\nu\left(x_{1,25}; \hat{\boldsymbol{\theta}}\right), g_\nu\left(x_{2,1}; \hat{\boldsymbol{\theta}}\right), g_\nu\left(x_{2,2}; \hat{\boldsymbol{\theta}}\right), \ldots, g_\nu\left(x_{2,25}; \hat{\boldsymbol{\theta}}\right), \ldots, g_\nu\left(x_{25,1}; \hat{\boldsymbol{\theta}}\right), g_\nu\left(x_{25,2}; \hat{\boldsymbol{\theta}}\right), \ldots, g_\nu\left(x_{25,25}; \hat{\boldsymbol{\theta}}\right)\right)^T$.

Instead of Tanimoto- type measure of similarity we will use also the following precision measure of analytical approximation:

$$R_3\left(\mathbf{A}, M_{1,\nu}\right) = \frac{1}{2}\left(1 + \frac{\boldsymbol{\alpha}^T\boldsymbol{\beta}}{|\boldsymbol{\alpha}| \cdot |\boldsymbol{\beta}|}\right), \quad (19)$$

$$R_3\left(\mathbf{A}, M_{2,\nu}\right) = \frac{1}{2}\left(1 + \frac{\boldsymbol{\alpha}^T\boldsymbol{\gamma}}{|\boldsymbol{\alpha}| \cdot |\boldsymbol{\gamma}|}\right). \quad (20)$$

Numerical analysis is used for the evaluation of approximation precision because analytical methods are not performing properly here. It is especially noticed during comparison of the results obtained using models $f_\nu\left(x, y; \hat{\boldsymbol{\theta}}\right)$ and corresponding models $g_\nu\left(x; \hat{\boldsymbol{\theta}}\right)$. Obviously, obtained numerical results (see histograms A,B,C; A',B',C'; A",B",C"; A'",B'",C'") fully confirm the theoretical expectation that approximation precision increases when the number of basis functions in a model is increased. This fact is confirmed by all chosen precision measures, calculated for the digital images of the first category. Despite the fact that the number of basis functions is enlarged nearly twice when the model case is changed to the next, obtained precision enhancement was not significant (Fig.1., see histograms A,B,C; A',B',C'; A",B",C"; A'",B'",C'").

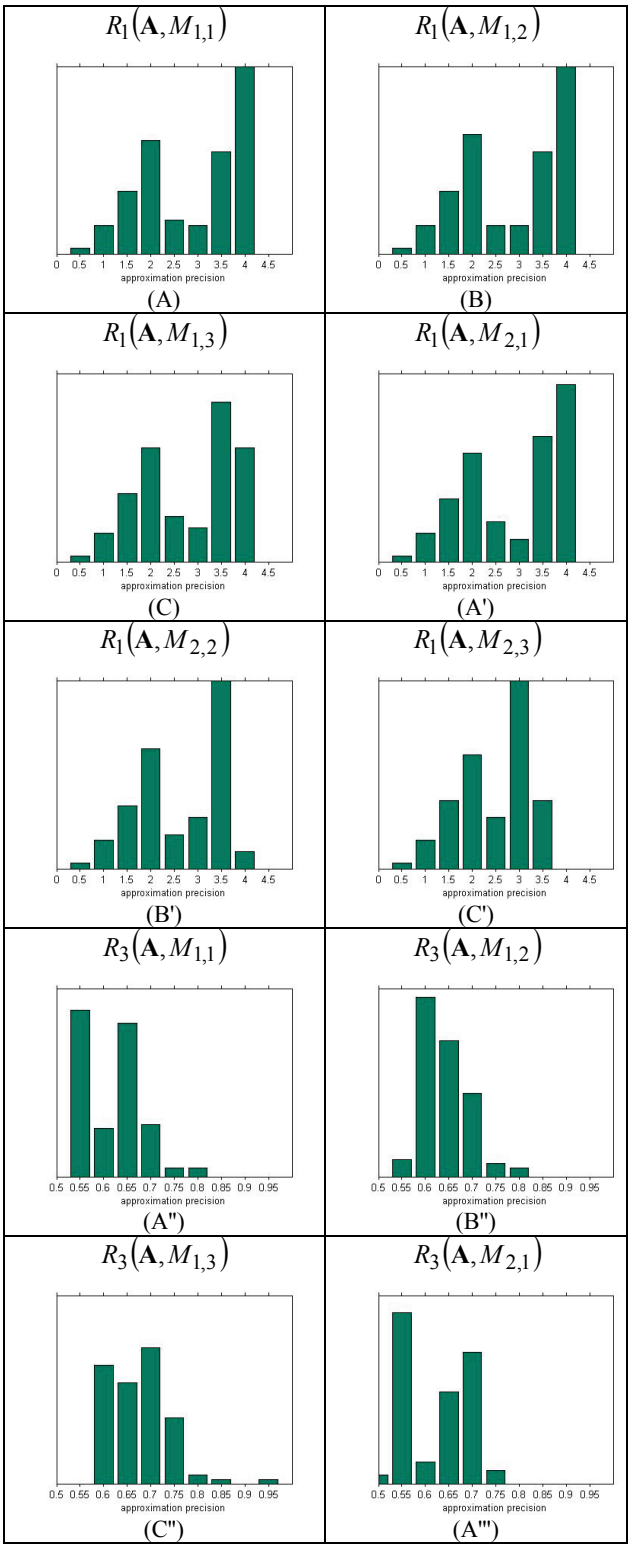

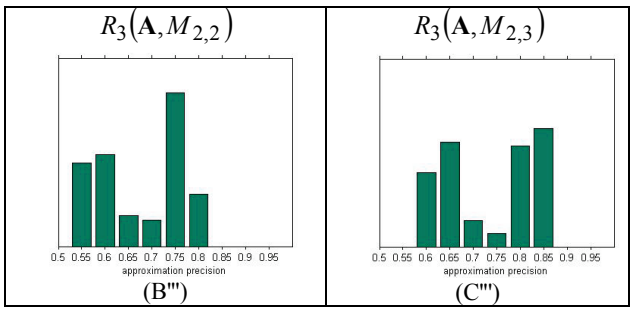

Fig. 1. Approximation precision histograms

It should be noticed that precision measures of model (1) are close to those for the same cases of model (2). However, a more careful analysis shows that, for the case of 49 functions, approximation precision of model (1) is noticeably better than that of the model (2).

In addition, it is noticed that the precision measure $R_1(\mathbf{A}, M_{\mu,\nu})$ can be used to get a certain idea about the mean approximation precision of a pixel by dividing $R_1(\mathbf{A}, M_{\mu,\nu})$ by the number of pixels 625. Table 2 shows lower and upper values of this measure for particular model / case.

Table 2. Precision boundary

Model	(4)	(5)	(6)	(4')	(5')	(6')
Lowest / Highest boundary	0.71 / 4.12	0.70 / 3.82	0.69 / 3.70	0.71 / 4.20	0.70 / 4.17	0.69 / 4.11

As histograms for the precision measure $R_2(\mathbf{A}, M_{\mu,\nu})$ turn out to be similar with histograms for the precision measure $R_3(\mathbf{A}, M_{\mu,\nu})$, only histograms for the precision measure $R_2(\mathbf{A}, M_{2,\nu})$ are presented in Fig.2. (see histograms D,E,F and compare them with A''', B''',C''', respectively).

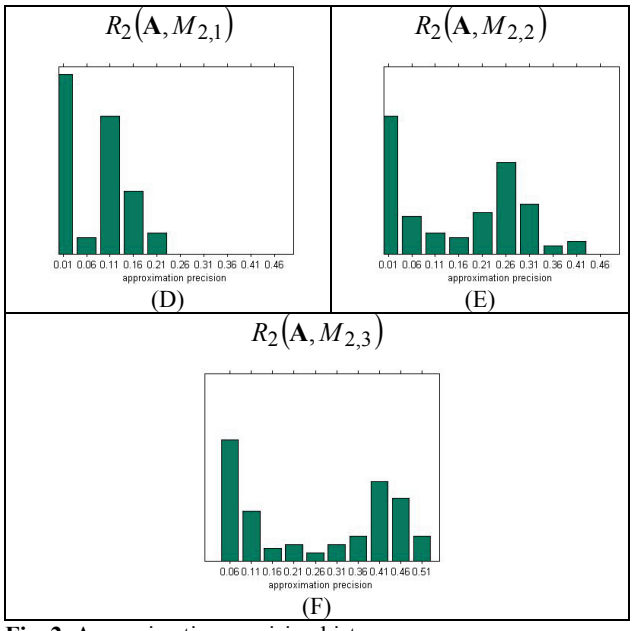

Fig. 2. Approximation precision histograms

Precision measures calculated for the digital images of the second category have shown very similar results.

Quality of image classification

All digital images of both categories can be divided into two subsets: those that "contain" (subset S_1) and "not contain" (subset S_2) foreign body to be identified. We will say that a digital image "contains" a foreign body if it is obtained by scanning the real scene where such a body is present. Classification problems discussed here are related to real application tasks.

Classification of images within one category is performed according to the scheme described in [1]. To implement that, non-empty subsets of images S_1' and S_2' of corresponding category were chosen. All images $\mathbf{A} \in S_1' \cup S_2'$ were transformed into vectors of coefficients $\hat{\boldsymbol{\theta}}$ of the chosen model and sets of vectors V_1' and V_2' representing corresponding images were formed.

As the next step, sets V_1' and V_2' were clusterized exploiting the full (complete) linkage rule of the hierarchic clustering. Clustering was stopped when 5 clusters were obtained. Centers of all clusters were calculated and sets of vectors V_1' and V_2' replaced by sets of calculated cluster centers Z_1' and Z_2'.

Image of the corresponding category was classified as "not containing" a foreign body, if

$$d_e(\hat{\boldsymbol{\theta}}, Z_1') \le d_e(\hat{\boldsymbol{\theta}}, Z_2'), \qquad (21)$$

where $\hat{\boldsymbol{\theta}}$ is a vector of coefficients representing image $\mathbf{A}$, and d_e is the Euclidian distance. It means that the result of classification is determined by the LRM used in the procedure, by exploited clustering procedure and Euclidian distance from the vector $\hat{\boldsymbol{\theta}}$ representing image $\mathbf{A}$ to the cluster centers Z_i'. It was expected that better classification results will be obtained when LRM with larger number of basis functions will be used. Numerical analysis using the training set $S' = S_1' \cup S_2'$ of size $|S'| = 100$ images of category 1, where $|S_1'| = 35$ and $|S_2'| = 65$, produced the following results. When 35 images from the set $S_1 \setminus S_1'$ were classified, number of errors was 5; when classifying 65 images from the set $S_2 \setminus S_2'$, number of errors was 0. Classification procedure exploited LRM $f_2(x, y; \boldsymbol{\theta})$.

Different and not easily explained results were obtained using the models $f_1(x, y; \boldsymbol{\theta})$ and $f_3(x, y; \boldsymbol{\theta})$. When 35 images from the set $S_1 \setminus S_1'$ were classified using the model $f_1(x, y; \boldsymbol{\theta})$, number of errors was 2; when classifying 65 images from the set $S_2 \setminus S_2'$, number of errors was 0. It means that results were better than in the case of 25 basis functions. Even stranger classification results were obtained for 49 basis functions, i.e. using LRM $f_3(x, y; \boldsymbol{\theta})$, the number of errors was correspondingly 10 and 0 in this case. Thus, a more precise approximation has lead to worse classification results.

If the classification was based on model $g_1(x;\boldsymbol{\theta})$, number of errors was correspondingly 3 and 0; with model $g_2(x;\boldsymbol{\theta})$ it was 7 and 0, but exploiting model $g_3(x;\boldsymbol{\theta})$ resulted in 5 and 0 errors.

For images of the second category where the glass objects had to be identified, the size $|S'|$ of the training set S' was 250, where $|S_1'|=125$ and $|S_2'|=125$. After that, 250 images were tested, which were not included in the training set, from those 125 contained glass objects and 125 did not.

Using models of the second type, the following classification results were obtained. If the approximation was based on functions $f_1(x,y;\hat{\boldsymbol{\theta}})$, there were 7 errors obtained from 125 images containing glass; with functions $f_2(x,y;\hat{\boldsymbol{\theta}})$ number of errors was 36; and with functions $f_3(x,y;\hat{\boldsymbol{\theta}})$ number of errors increased up to 82. In all cases there were no errors in classification of images that did not contain glass. Explanation of these results remains an open problem. The hypothesis was advanced that erroneous results are obtained due to a loss of information in clustering process of vector sets V_1' and V_2' when clusters are replaced by their centers. To check that, classification was performed using the Fix- Hodges principle [4] with parameter $q=15$. However, classification quality practically was not improved using this method. Therefore this hypothesis was rejected. Then, to find the cause, Euclidian distance d_e used to derive the classification decision was replaced by Jordan's or Chebyshev's distance d_j. Numbers of classification errors are illustrated in Table 3.

Table 3. Classification error

Approximation function	Classification error
$f_1(x,y;\hat{\boldsymbol{\theta}})$	$(4;0)_j$
$f_2(x,y;\hat{\boldsymbol{\theta}})$	$(43;0)_j$
$f_3(x,y;\hat{\boldsymbol{\theta}})$	$(75;2)_j$

Here, $f_v(x,y;\hat{\boldsymbol{\theta}})$ indicates the LRM used, and the corresponding pair of numbers in brackets show the number of errors of the first and second type, assuming that erroneous classification of the image containing the object is the error of the first type.

By changing the decision- making rule, i.e. replacing the nearest neighbour principle with condition

$$d_j(\hat{\boldsymbol{\theta}},Z_1)-d_j(\hat{\boldsymbol{\theta}},Z_2)<0.004, \qquad (22)$$

quality of the classification was noticeably improved (Table 4).

Table 4. Classification error

Approximation function	Classification error
$f_1(x,y;\hat{\boldsymbol{\theta}})$	$(0;3)_j$
$f_2(x,y;\hat{\boldsymbol{\theta}})$	$(1;3)_j$
$f_3(x,y;\hat{\boldsymbol{\theta}})$	$(29;3)_j$

The fact that also in this case the more precise approximation model provided worse results is still difficult to explain.

Conclusions

Numerical analysis clearly shows that linear regression method cannot be used for solving the practical tasks of image classification in a pure formal way; different components of this method should be experimentally evaluated to choose the most appropriate LRM, clustering procedure, distance measure and decision rule. We notice that increased approximation precision of the model does not imply increased classification quality. Unexpected classification results for the images of the second category force us to conclude that forming of the adequate training set is important for obtaining the proper solution. That most directly is related to subset S_1'. In addition, it may not be assumed that the regression method is well suited for classification of all types of digital images.

References

1. **Lorencs A., Mednieks I., Sinica-Sinavskis J.** Fast Object Detection in Digital Grayscale Images // Proceedings of the Latvian Academy of Sciences. – 2009. – Vol. 63. – P. 116–124.
2. **Лоренц А. А.** Многомерные планы наблюдений, индуцирующие невырожденность информационных матриц регрессионных моделей // Автоматика и вычислительная техника. – 2010. – No. 2.
3. **Натансон И. П.** Конструктивная теория функций. – Москва, 1949. – 688 с.
4. **Fix E., Hodges J. L.** Discriminatory Analysis, Nonparametric Discrimination // Report Number 11. Project Number 21-49-004, USAF School of Aviation Medicine, Randolph Field, Texas. – 1951. – P. 261–279.

Received 2010 02 18

A. Lorencs, J. Sinica-Sinavskis. One Method of Image Processing and its Numerical Analysis // Electronics and Electrical Engineering. – Kaunas: Technologija, 2010. – No. 7(103). – P. 25–30.

The paper discusses application of linear regression models to image transformation and pattern recognition, oriented towards creation of technology for fast processing of digital images. Theoretical and heuristic expectations are confronted with results of numerical analysis. Digital images are considered to be sets of samples taken from the surface of brightness levels. Adequate regression models, i.e. analytic expressions of functions for representation of these surfaces are sought. Images are represented by vectors of

coefficients of the model calculated using the least squares method. Classification of images further is based on classification results of coefficient vectors of linear regression models. Ill. 2, bibl. 4, tabl. 4 (in English; abstracts in English, Russian and Lithuanian).

А. Лоренц, Ю. Синица-Синявскис. Об одном методе обработки изображений и его численном анализе // Электроника и электротехника. – Каунас: Технология, 2010. – № 7(103). – С. 25–30.

Исследуются способы использования линейных регрессионных моделей для преобразования изображений и их распознавания, направленные на развитие технологий быстрой обработки дискретных изображений. Теоретические и эвристические прогнозы сопоставлены с результатами численного анализа. Дискретное изображение рассматривается как выборка определенного множества апликат точек поверхности яркостей. Предлагаются подходящие регрессионные модели, т. е. аналитические выражения для функций, представляющих эти поверхности. Изображения представляются векторами коэффициентов линейных регрессионных моделей, вычисленных по методу наименьших квадратов. Классификация изображений далее основывается на результатах классификации векторов коэффициентов, соответствующих линейным регрессионным моделям. Ил. 2, библ. 4, табл. 4 (на английском языке; рефераты на английском, русском и литовском яз.).

A. Lorencs, J. Sinica-Siniavskis. Skaitmeninis informacijos apdorojimo metodas // Elektronika ir elektrotechnika. – Kaunas: Technologija, 2010. – Nr. 7(103). – P. 25–30.

Aprašoma nauja informacijos apdorojimo technologija, paremta euristiniu prognozavimu ir skaitmenine rezultatų analize. Pasiūlyti regresiniai modeliai, kuriuose naudojami vektoriniai koeficientai ir apskaičiuojami mažiausių kvadratų metodai. Pasiūlyta originali technologija, kurioje rezultatai klasifikuojami. Koeficientų vektoriai leidžia optimaliai taikyti tiesinius regresinius informacijos apdorojimo modelius. Il. 2, bibl. 4, lent. 4 (anglų kalba; santraukos anglų, rusų ir lietuvių k.).

DOI: 10.5755/j02.eie.9269